ISSN 0030-400X, Optics and Spectroscopy, 2021, Vol. 129, No. 12, pp. 1300–1305. © Pleiades Publishing, Ltd., 2021.
ISSN 0030-400X, Optics and Spectroscopy, 2021. © Pleiades Publishing, Ltd., 2021.
Russian Text © The Author(s), 2021, published in Optika i Spektroskopiya, 2021, Vol. 129, No. 9, pp. 1176–1181.

The Influence of Polyvinylpyrrolidone on the Structure and Optical Properties of ZnO–MgO Nanocomposites Synthesized by the Polymer–Salt Method

A. A. Shelemanov[a, *], R. K. Nuryev[a], S. K. Evstropiev[a, b, c], V. M. Kiselev[b], and N. V. Nikonorov[a]

[a] *ITMO University, St. Petersburg, 197101 Russia*

[b] *Vavilov State Optical Institute, St. Petersburg, 192171 Russia*

[c] *St. Petersburg State Institute of Technology (Technical University), St. Petersburg, 190013 Russia*

**e-mail: shelemanov@mail.ru*

Received February 1, 2021; revised February 1, 2021; accepted February 3, 2021

Abstract—The influence of polyvinylpyrrolidone on the structure and optical properties of ZnO–MgO nanocomposites synthesized by the polymer–salt method is studied. The synthesized nanocomposites are studied by the methods of optical and luminescence spectroscopy and X-ray diffraction analysis. An increase in the polyvinylpyrrolidone concentration in solutions leads to a decrease in the size of forming ZnO crystals, an increase in the luminescence intensity of ZnO–MgO nanocomposites in the blue spectral region, and quenching of luminescence at longer wavelengths. The efficiency of singlet oxygen photogeneration by ZnO–MgO nanocomposites obtained by the polymer–salt method increases with increasing concentration of polyvinylpyrrolidone in initial solutions.

Keywords: luminescence, spectra, crystals, ZnO, singlet oxygen

DOI: 10.1134/S0030400X21090198

INTRODUCTION

The ZnO–MgO solid solutions are wide gap semiconductor materials (E_g ~ 3–5 eV) [1, 2] with a high transparency in the UV region and high chemical resistance and hardness. The atomic sizes of Mg and Zn and the lengths of the Mg–O and Zn–O bands are close to each other [3–8], which leads to low defectness of the structure of composites based on these oxides and makes them promising for developing various quantum-size heterostructures for modern optics, optoelectronics, and electronics. A high efficiency of chemically-active singlet oxygen generation by photoactive ZnO–MgO nanocomposite layers in microcapillary optical elements was shown in [9].

The structure and optical properties of ZnO–MgO nanomaterials obtained by different methods were studied in a number of works [10–16]. In [9, 10], the ZnO–MgO nanomaterials were synthesized by the polymer–salt method with the use of polyvinylpyrrolidone (PVP) as a stabilizing component. This soluble polymer, which is widely used for stabilization in solutions of various nanoparticles [17–24], chemically interacts and forms complexes with nanoparticles [21–23], iodine [25], and metal ions (Zn^{2+}, Ag^{+}, Co^{2+}, Ni^{2+}) [26–28].

In addition to the stabilizing effect on nanoparticles forming in solution, PVP provides high adhesion to surfaces of various materials [10, 29, 30] and participates in oxidation–reduction processes occurring in solution [18, 21] or solid materials upon their thermal treatment during the polymer–salt synthesis [31]. Detailed study of the influence of PVP on the structure and properties of optical materials and coatings is important for biomedical and ecological optical applications.

The aim of the present work is to study the influence of the PVP concentration on the structure and optical properties of MgO–ZnO nanomaterials synthesized by the liquid polymer–salt method, as well on their ability to photogenerate chemically-active oxygen.

EXPERIMENTAL

As initial components, we used aqueous solutions of $Zn(NO_3)_2$, $Mg(NO_3)_2$, and PVP (M_w = 1300000, Sigma-Aldrich). After mixing at room temperature, the solutions were used for deposition of coatings on samples of alkali-silicate glasses and for formation of PVP–metal nitrate composites by drying.

After drying at 70°C, the materials were thermally treated at 550°C for 2 h, which caused complete decomposition of PVP and metal salts and formation of oxide coatings on glasses or dispersed oxide pow-

Table 1. Chemical composition of materials

Sample	Chemical composition of solutions, wt %					Chemical composition of powders, wt %	
	H_2O	PVP	Alcohol	$Zn(NO_3)_2 \cdot 6H_2O$	$Mg(NO_3)_2 \cdot 6H_2O$	ZnO	MgO
100	51.916	2.596	40.962	4.077	0.449	90.909	9.091
50	52.599	1.315	41.501	4.131	0.455		
25	52.947	0.662	41.775	4.158	0.468		
0	53.300	0	42.054	4.186	0.461		

ders. Table 1 presents the chemical compositions of the used solutions and obtained oxide materials.

X-ray diffraction analysis of materials was performed using a Rigaku Ultima IV diffractometer.

The absorption spectra of materials were measured on a Rigaku Ultima IV LAMBDA 650 spectrophotometer. The band gap of coating materials was determined using the Tauc equation [32]

$$(\alpha h\nu)^2 = A(h\nu - E_g), \quad (1)$$

where $h\nu$ is the photon energy, E_g is the band gap of the semiconductor, A is a constant, and α is the absorption coefficient. By plotting graphs in coordinates $(\alpha h\nu)^2 = f(h\nu)$, we can determine E_g in the materials studied.

The photoluminescence of powders was measured on a Perkin Elmer LS-50B fluorescence spectrophotometer in the range of 400–650 nm under excitation at $\lambda_{ex} = 370$ nm.

It is known that chemically-active singlet oxygen under action of external radiation demonstrates characteristic luminescence in the near-IR spectral region ($\lambda_{max} = 1270$ nm) [9, 33–35]. To study singlet oxygen photogeneration by the synthesized materials, we used the experimental setup described in detail in [8]. The luminescence was excited by light-emitting diodes of the HPR40E-50UV series ($\lambda_{max} = 370$ nm, power density 0.35 W/cm^2 and $\lambda_{max} = 405$ nm, power density 0.90 W/cm^2).

EXPERIMENTAL RESULTS AND DISCUSSION

Figure 1 shows the diffraction patterns of ZnO–MgO materials obtained from solutions without silver. The diffraction patterns clearly show multiple peaks of hexagonal ZnO crystals with the wurtzite structure (JCPDS 36-1451) and low-intensity peaks of cubic MgO crystals (periclase) (JCPDS 45-0946). The intensity ratios of different ZnO peaks are close to the standard values (JCPDS 36-1451).

Based on the data obtained, we determined the average sizes of ZnO crystals in oxide composites (Fig. 2) and their crystal lattice parameters (Table 2).

Figure 2 shows the dependence of the average size of ZnO crystals in oxide composites on the PVP concentration in the initial mixtures. An increase in the PVP concentration in initial mixtures leads to a decrease in the size of ZnO crystals in ZnO–MgO composites. This effect is most pronounced with adding the first PVP portions.

The low intensity of the MgO peaks observed in the diffraction patterns (Fig. 1) testify to a low concentration of periclase crystals in the composites. Table 2 shows that the ZnO lattice cell parameters in the composites are considerably smaller than the standard values (JCPDS 36–1451). The Mg^{2+} ionic radius (0.65 Å according to Pauling) is smaller than the Zn^{2+} radius (0.74 Å according to Pauling). Because of this, the substitution of Zn^{2+} ions by Mg^{2+} in sites of the zinc oxide crystal lattice can be accompanied by some deformation and a decrease in the ZnO unit cell parameters. Based on the data of Fig. 1 and Table 2, we can suppose that some amount of Mg^{2+} ions isomorphously substitute Zn^{2+} in the crystal lattice of zinc oxide. We can also note a tendency to an increase in V_{ZnO} with increasing PVP concentration in the initial mixtures (Table 2).

Figure 3 presents the absorption spectrum of a glass sample with ZnO–MgO coating. Experiments showed that a change in the PVP concentration in the initial solutions almost did not affect the shape of absorption spectra of these samples. The absorption spectra

Table 2. Parameters of the ZnO lattice cell in ZnO–MgO composites obtained

Sample	ZnO lattice cell parameters		
	a, b, Å	c, Å	V_{ZnO}, Å^3
0	3.2369	5.1903	47.097
25	3.2399	5.1770	47.063
50	3.2423	5.1801	47.160
100	3.2438	5.1818	47.219
JCPDS 01-070-8072	3.2465	5.2030	47.491

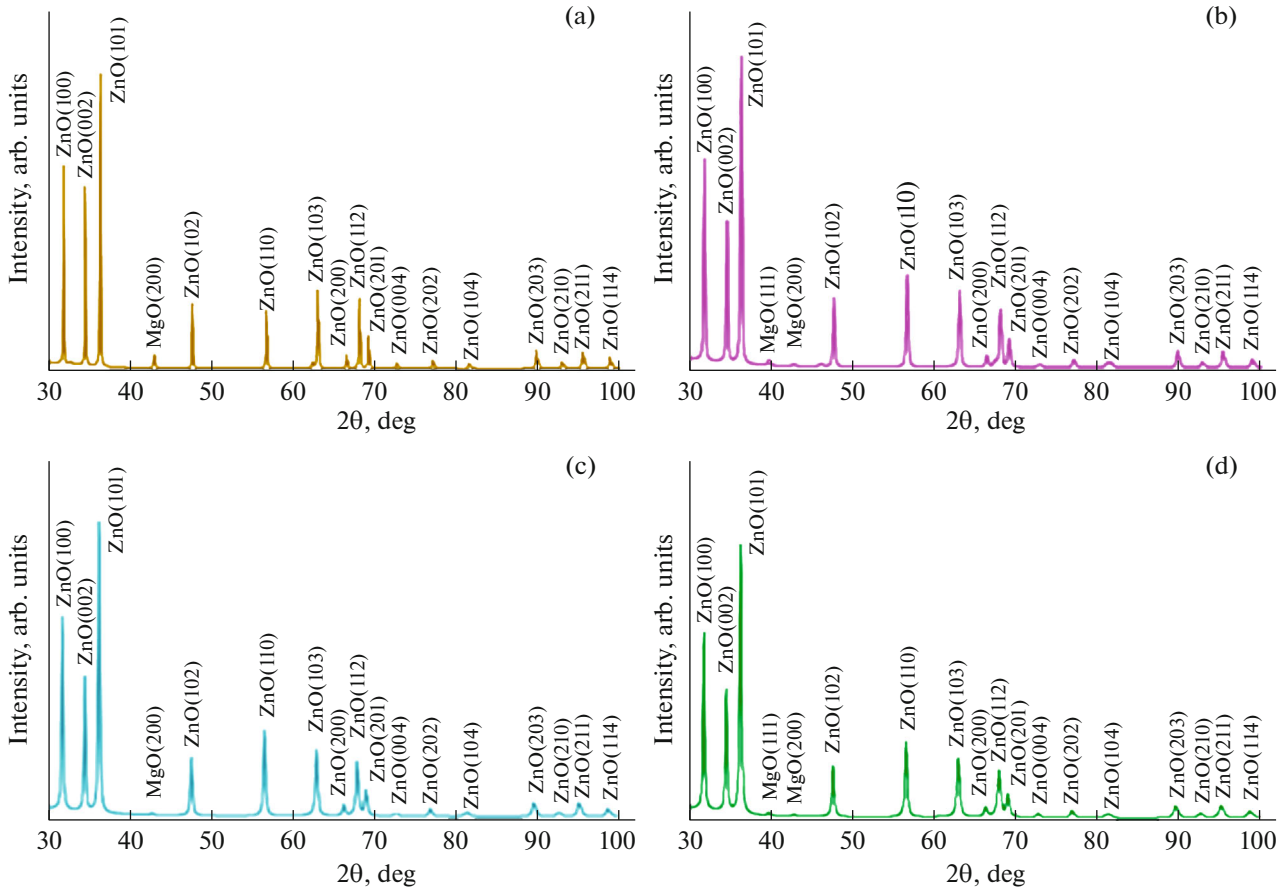

Fig. 1. Diffraction patterns of ZnO–MgO samples (a) 0, (b) 25, (c) 50, and (c) 100 synthesized from solutions with different PVP concentrations.

glasses with ZnO–MgO coatings show bends in the range of 340–350 nm related to the exciton absorption band of zinc oxide nanoparticles.

It was experimentally shown in [2, 10, 11, 14] that the band gap of MgO/ZnO materials obtained by different methods increases with increasing MgO con-

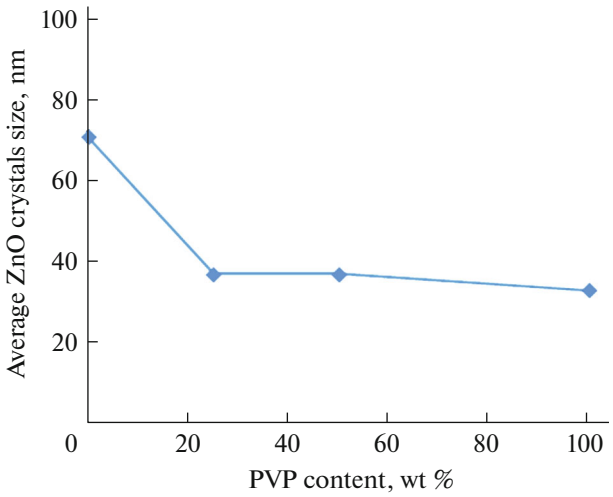

Fig. 2. Dependence of the average size of ZnO crystals on the PVP concentration in the initial solutions.

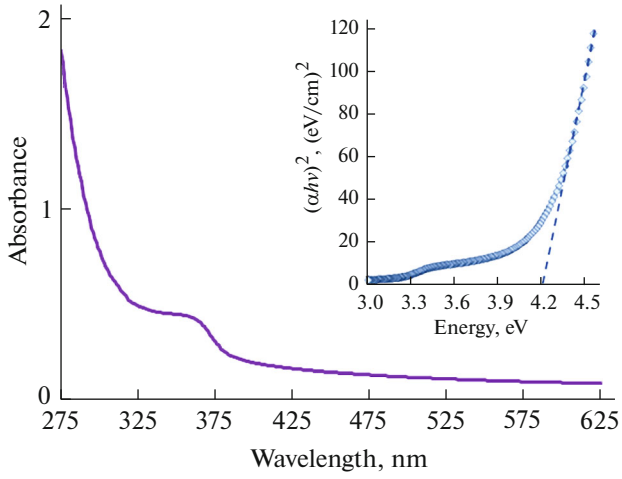

Fig. 3. Absorption spectrum of glass with a ZnO–MgO coating obtained from solution 125–50. The inset shows dependence $(\alpha h\nu)^2 = f(h\nu)$ for the ZnO–MgO coating.

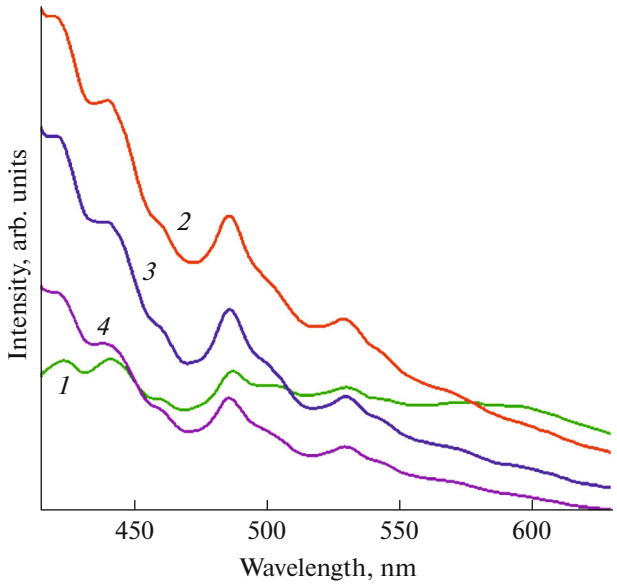

Fig. 4. Photoluminescence spectra of ZnO–MgO powders synthesized from solutions with different PVP concentrations for samples (*1*) 0, (*2*) 25, (*3*) 50, and (*4*) 100.

centration. The inset in Fig. 3 shows dependence $(\alpha h\nu)^2 = f(h\nu)$ for the ZnO–MgO coating. Calculations of E_g^{ef} showed that the band gap of the synthesized coatings is 4.2–4.3 eV and almost does not change with variations in the PVP concentration in initial solutions. These values of E_g^{ef} noticeably exceed the band gap of ZnO (3.4 eV [36]) and almost coincide with the band gap of ZnO–MgO materials obtained previously by molecular beam epitaxy [8] and a liquid method [10].

Figure 4 presents the photoluminescence spectra (λ_{ex} = 370 nm) of ZnO–MgO powders synthesized from solutions with different PVP concentrations. The spectra exhibit luminescence bands typical for different ZnO defect centers described in [37–40]. It is seen that PVP additives in the initial solutions strongly affect the intensity ratios of luminescence bands. The introduction of PVP into the solutions leads to enhancement of luminescence in the blue spectral region and to suppression of luminescence at longer wavelengths. Further increase in the PVP concentration is solutions leads to a decrease in the luminescence intensity in the entire visible spectral region.

The study of solutions containing ZnO nanoparticles synthesized in solutions with PVP showed [24] that the luminescence intensity of ZnO nanoparticles in the UV spectral region considerably increases in the presence of PVP molecules. Simultaneously, the characteristic visible luminescence of various ZnO defect centers is considerably suppressed. The authors of [24] explain this effect by a high level of passivation of the surface of zinc oxide nanoparticles by PVP molecules.

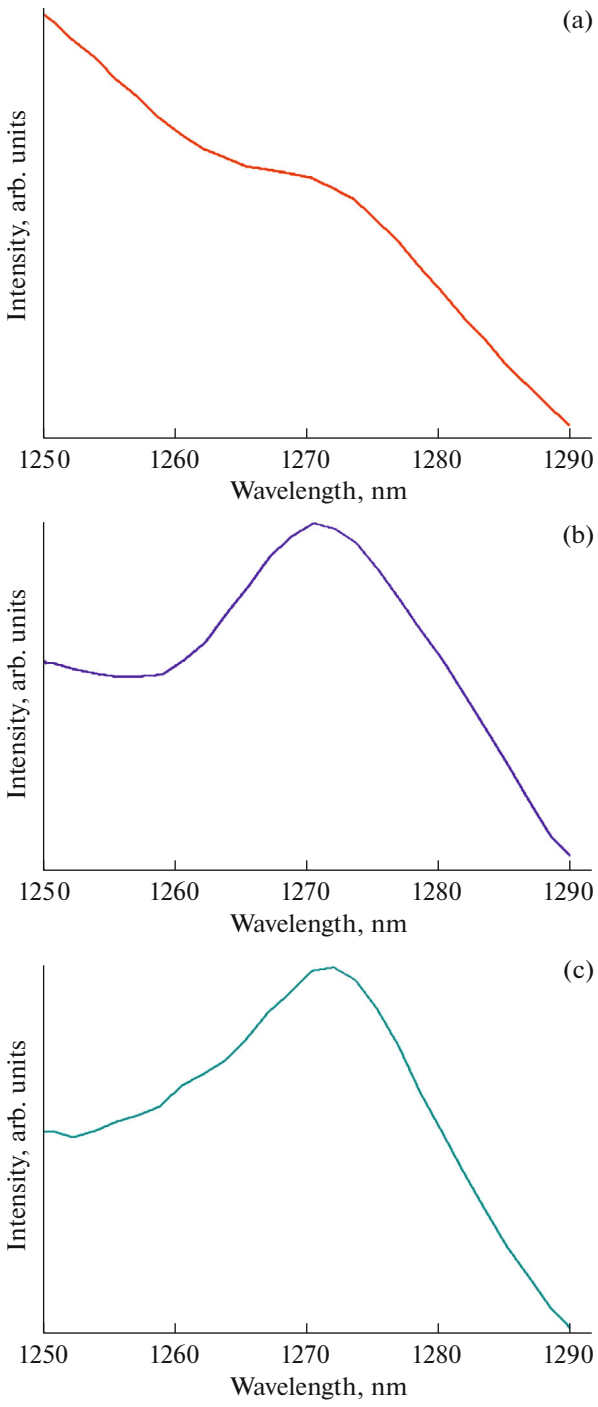

Fig. 5. Photoluminescence spectra (λ_{ex} = 370 nm) of ZnO–MgO coatings with different PVP concentrations (samples (a) 0, (b) 25, and (c) 50).

Thus, it can be noted that the influence of PVP on the luminescent properties of ZnO nanoparticles is similar in the case of their formation in solutions at room temperature and in the case of synthesis by the used polymer–salt method with thermal treatment.

Figure 5 shows the photoluminescence spectra in the range of 1250–1290 nm for ZnO–MgO composites synthesized from solutions with different PVP concentrations. One can see that the spectra contain the singlet oxygen absorption band peaking at λ_{max} = 1270 nm, which is characteristic of the $^1\Delta_g$–$^3\Sigma_g$ electronic transition [33–35]. Addition of PVP to the initial solutions leads to a noticeable increase in the intensity of this band.

It is known that chemically-active oxygen generation occurs on the surface of materials. A decrease in the size of ZnO crystals in powders with introduction of PVP into the initial solutions (Fig. 2) is accompanied by an increase in their specific surface and is to a large extent responsible for an increase in the singlet oxygen generation efficiency.

CONCLUSIONS

The introduction of PVP into the initial solutions used for the polymer–salt synthesis of ZnO–MgO nanocomposites considerably affects their crystal structure and optical properties. An increase in the concentration of this polymer in solutions leads to a decrease in the size of formed ZnO crystals, to an increase in the luminescence intensity of ZnO–MgO nanocomposites in the blue spectral region, and to suppression of the luminescence in the long-wavelength region. The efficiency of singlet oxygen photogeneration by ZnO–MgO nanocomposites synthesized by the polymer–salt method increases with increasing PVP concentration in the initial solutions.

FUNDING

This work was partially (Evstropiev S.K.) supported by the Russian Foundation for Basic Research (project no. 19-19-00596).

CONFLICT OF INTEREST

The authors declare that they have no conflict of interest.

REFERENCES

1. A. J. Skinner and J. P. Lafemina, Phys. Rev. B **45**, 3557 (1992).
2. O. Madelung, M. Schulz, and H. Weiss, in *Landolt–Börnstein Group III Condensed Matter* (Springer, Berlin, 2008), Vol. 44, Subvol. B.
3. E. Clementi, D. L. Raimondi, and W. P. Reinhardt, *Atomic Screening Constants from SCF Functions. II. Atoms with 37 to 86 Electrons* (Reinhold, New York, 1962).
4. L. E. Sutton, *Supplement 1956–1959, Spec. Publ. No. 18, Table of Interatomic Distances and Configuration in Molecules and Ions* (R. Chem. Soc., London, 1965).
5. J. E. Huheey, E. A. Keiter, and R. L. Keiter, *Inorganic Chemistry: Principles of Structure and Reactivity,* 4th ed. (Harper Collins, New York, 1993).
6. W. W. Porterfield, *Inorganic Chemistry, A Unified Approach* (Addison-Wesley, Reading MA, 1984).
7. A. M. James and M. P. Lord, *MacMillan's Chemical and Physical Data* (Macmillan, Basingstoke, 1992).
8. S. Fujita, H. Tanaka, and S. Fujita, J. Cryst. Growth **278**, 264 (2005).
9. I. V. Bagrov, V. M. Kiselev, S. K. Evstropiev, A. S. Saratovskii, V. V. Demidov, and A. S. Matrosova, Opt. Spectrosc. **128**, 214 (2020).
10. S. K. Evstropiev, L. P. Soshnikov, and E. V. Kolobkova, Opt. Mater. **203**, 133 (2018).
11. S. Choopun, R. D. Vispute, W. Yang, and R. P. Sharma, Appl. Phys. Lett. **80**, 1629 (2002).
12. L. Srinivasa Rao, T. Venkatappa Rao, and S. Naheed, Mater. Chem. Phys. **203**, 133 (2018).
13. N. Eker, A. Balta, Ö. Ertek, and İ. Okur, Mater. Sci. Appl. **6**, 40 (2015).
14. N. Nishimoto, K. Yoshino, J. Fujihara, and K. Kitahara, e-J. Surf. Sci. Nanotech. **13**, 185 (2015).
15. K. Vijayalakshmi and K. Karthick, J. Hydrogen Energy **39**, 7165 (2014).
16. M. Caglar, J. Wu, and K. Li, Mater. Res. Bull. **45**, 284 (2010).
17. I. V. Bagrov, V. V. Danilov, S. K. Evstrop'ev, V. M. Kiselev, I. M. Kislyakov, A. S. Panfutova, and A. I. Khrebtov, Tech. Phys. Lett. **81**, 65 (2015).
18. S. K. Evstropiev, N. V. Nikonorov, and A. Saratovskii, J. Photochem. Photobiol., A **403**, 112858 (2020).
19. K. M. Koczkur, S. Mourdikoudis, and L. Polavarapu, Dalton Trans. **44**, 17883 (2015).
20. K. S. Evstrop'ev, Yu. A. Gatchin, and S. K. Evstrop'ev, Opt. Spectrosc. **120**, 415 (2016).
21. C. Kan, W. Cai, C. Li, and L. Zhang, J. Mater. Res. **20**, 320 (2005).
22. Z. Ying, L. Jing-Ying, M. Song, and Z. Ya-Jing, Mater. Sci.: Mater. Med. **21**, 1205 (2010).
23. Z. Zhang, B. Zhao, and L. Hu, Solid State Chem. **121**, 105 (1996).
24. L. Guo, S. Yang, and C. Yang, Appl. Phys. Lett. **76**, 2901 (2000).
25. M. Nasreen, M. L. Chikindas, and K. Uhrich, Appl. Polym. Sci. **117**, 329 (2010).
26. N. A. Volkova, S. K. Evstropiev, N. V. Nikonorov, and K. S. Evstropyev, Opt. Spectrosc. **127**, 738 (2019).
27. K. V. Anasuya, M. K. Veeraiah, and S. Prasannakumar, Adv. Chem. Sci. **2**, 12 (2014).
28. K. V. Anasuya, M. K. Veeraiah, P. Hemalatha, and M. Manju, J. Appl. Chem. **7** (8), 21 (2014).
29. H. Kozuka, M. Kajimura, T. Hirano, and K. Katayama, J. Sol-Gel Sci. Technol. **19**, 205 (2000).

30. C. Jing, J. Hou, Y. Zhang, and X. Xu, J. Non-Cryst. Solids **353**, 4128 (2007).

31. E. V. Kolobkova, S. K. Evstropiev, N. V. Nikonorov, V. N. Vasilyev, and K. S. Evstropiev, Opt. Mater. **73**, 712 (2017).

32. J. Tauc, Mater. Res. Bull. **3**, 37 (1968).

33. A. A. Krasnovsky and R. V. Ambartzumian, Chem. Phys. Lett. **400**, 531 (2004).

34. Y. Li, W. Zhang, and J. Niu, ACS Nano **6**, 5164 (2012).

35. V. M. Kiselev, S. K. Evstrop'ev, and A. M. Starodubtsev, Opt. Spectrosc. **123**, 809 (2017).

36. D. C. Reynolds, D. C. Look, B. Jogai, and C. W. Litton, Phys. Rev. B **60**, 2340 (1999).

37. S. Dey and A. K. Mishra, in *Solid State Physics, Proceeding of the 55th DAE Solid State Physics Symposium 2010,* AIP Conf. Proc. **1349**, 319 (2011).

38. T. Chitradevi, A. J. Lenus, and N. V. Jaya, Mater. Res. Express **7**, 015011 (2020).

39. S. Bhattacharyya and A. Gedanken, Phys. Chem. **112**, 659 (2008).

40. P. A. Rodnyi, K. A. Chernenko, and I. D. Venevtsev, Opt. Spectrosc. **125**, 372 (2018).

Translated by M. Basieva